Molecular Vibrations at a Liquid−Liquid Interface Observed by Fourth-Order Raman Spectroscopy

Satoru Fujiyoshi,*,†,§ Taka-aki Ishibashi,‡,§ and Hiroshi Onishi†,§

Department of Chemistry, Faculty of Science, Kobe University, Nada, Kobe 657-8501, Japan; Department of Chemistry, Graduate School of Science, Hiroshima University, Kagamiyama, Higashi-Hiroshima 739-8526, Japan; and Core Research for Evolutional Science and Technology, Japan Science and Technology Agency, Honmachi, Kawaguchi 332-0012, Japan

Received: January 22, 2006; In Final Form: March 8, 2006

Interface-selective, Raman-based observation of molecular vibrations is demonstrated at a liquid−liquid interface. An aqueous solution of oxazine 170 dye interfaced with hexadecane is irradiated with pump and probe light pulses of 630-nm wavelengths in 17-fs width. The ultrashort pulses are broadened due to group velocity dispersion when traveling through the hexadecane layer. The dispersion is optically corrected to give an optimized instrumental response. The pump pulse induces a vibrational coherence of the dye via impulsive stimulated Raman scattering. The probe pulse generates second-harmonic light at the interface. The efficiency of the generation is modulated as a function of the pump−probe delay by the coherently excited molecules. Fourier transformation of the modulated efficiency presents the frequency spectrum of the vibrations. Five bands are recognized at 534, 557, 593, 619, and 683 cm^{-1}. The pump-and-probe process induces a fourth-order optical response that is forbidden in a centrosymmetric media. The contribution of an undesired, cascaded optical process is quantitatively considered and excluded.

1. Introduction

Liquid−liquid interfaces, including membranes and micelles, play a key role in a broad range of chemistry from biochemistry to chemical engineering. Interface-selective observation of molecular vibrations, which is not fully achieved at a liquid−liquid interface, provides rich information about the composition and structure of these interfaces. Sum-frequency generation (SFG) due to a second-order optical response, $\chi^{(2)}$, is a powerful tool to observe vibrations at interfaces open to vapor environments.[1−10] A target interface is irradiated with visible and infrared (IR) light pulses, and the light having a sum frequency of the visible and IR frequencies is generated. The intensity of the SFG light as a function of the IR frequency provides a vibrational spectrum. The efficiency of SFG is enhanced when IR photon energy comes in resonance with the vibrational transitions. Even-order optical response, $\chi^{(2,\ 4,\ldots)}$ is forbidden in any media with inversion symmetry, but necessarily allowed at an interface where the symmetry is certainly broken.[2,4] The SFG technique is therefore successful in probing open interfaces. Infrared light is, however, strongly absorbed by most liquids, especially by water. Access to interfaces buried in liquids is limited, while it is possible by irradiating probe light from the side of a weak IR-absorptive material.[5,7,11] An IR-free method of observation is necessary to provide full access to liquid−liquid interfaces.

We propose a Raman-based, fourth-order optical spectroscopy for this purpose. Solid and liquid surfaces open to air or vacuum have been observed with this method based on fourth-order response, $\chi^{(4)}$.[12−18] Successful application to a liquid−liquid interface is not trivial, though. Sub-20-fs light pulses are required to cause a higher optical process, fourth-order Raman response. When the pulses travel through a liquid layer covering the interface, the time width is broadened due to group velocity dispersion (GVD). The instrumental response in the time domain is hence perturbed, and the observable range of vibrational frequency may be limited. In the present study, the GVD is corrected to optimize the instrumental response.

2. Optical Transitions of Interest

Interface-selective, fourth-order Raman scattering and bulk-sensitive third-order Raman scattering are compared in Figure 1a. Molecules at an interface and also in bulk are vibrationally excited by a pump light pulse having a center frequency Ω and a wave vector $\boldsymbol{k}_{\mathrm{pump}}$. The frequency width of the pulse is related to the Fourier transformation (FT) of the time width, 900 cm^{-1} for a 17-fs pulse. Raman-active modes of vibration are excited via impulsive stimulated Raman scattering, when the frequency width exceeds the energy gap between the vibrational ground state g and the excited state v of the molecules. The vibrational coherence of $|g\rangle\langle v|$ and $|v\rangle\langle g|$ is thereby induced by the ultrafast pump irradiation. The efficiency of the coherent excitation is enhanced when an electronic transition from g to an electronic state e_1 is resonant to the pump photon energy $\hbar\Omega$.

At a time delay of t_d, a probe pulse having of a frequency Ω and a wave vector $\boldsymbol{k}_{\mathrm{probe}}$ interacts with the coherently excited molecules to generate signal light of 2Ω frequency. This pump-and-probe process contains four incident electric fields, and the signal field E_{fourth} is proportional to a fourth-order optical response, $\chi^{(4)}(t_d)$. The even-order optical process ensures the interface-selective observation of the vibrational coherence.[14,16] In our experiments, the fourth-order field is emitted to the

* Corresponding author. E-mail: fujiyoshi@phys.titech.ac.jp. Present address: Department of Physics, Tokyo Institute of Technology, Meguro, Tokyo 152-8551, Japan.

† Department of Chemistry, Faculty of Science, Kobe University.

‡ Department of Chemistry, Graduate School of Science, Hiroshima University.

§ Core Research for Evolutional Science and Technology, Japan Science and Technology Agency.

10.1021/jp060457g CCC: $33.50
Published on Web 04/26/2006

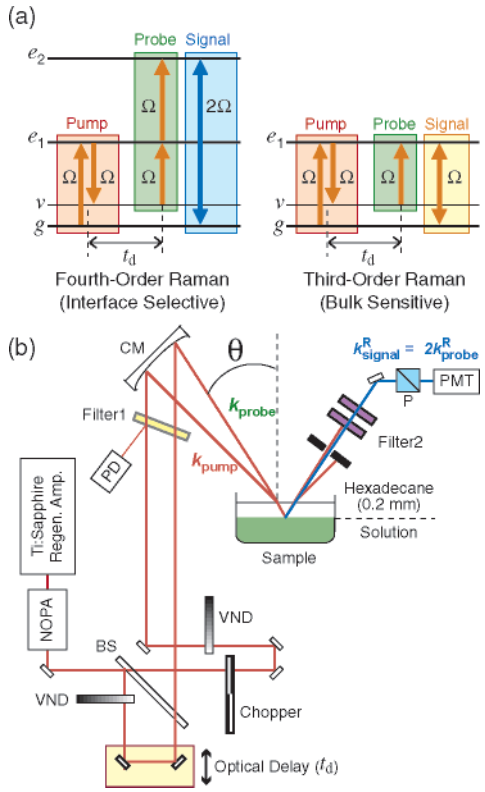

Figure 1. (a) Diagrams of fourth-order Raman and third-order Raman responses. (b) The fourth-order Raman spectrometer with NOPA, noncollinear optical parametric amplifier; BS, beam splitter; VND, variable neutral density filter; CM, concave mirror; PD, photodiode to check the pump on/off; P, Glan−Taylor polarizing prism; PMT, photomultiplier tube.

reflected direction with $\boldsymbol{k}^{R}_{signal} = \boldsymbol{k}^{R}_{pump} - \boldsymbol{k}^{R}_{pump} + 2\boldsymbol{k}^{R}_{probe}$, as illustrated in Figure 1b ($\boldsymbol{k}^{R}_{pump}$ and $\boldsymbol{k}^{R}_{probe}$ denote the wave vectors of the pump and probe lights reflected on the target interfaces). The third-order response, $\chi^{(3)}(t_d)$, is observed when the reflected probe light of the frequency Ω is acquired instead of 2Ω light. The whole portion of the molecules interacting with the pump and probe pulses contribute to generate the odd-order response, leading to bulk-sensitive detection of the vibrational coherence.

The fourth-order Raman field E_{fourth} due to $\chi^{(4)}(t)$ as a function of the pump−probe delay t_d is presented as the sum of periodic oscillations decayed exponentially

$$E_{fourth}(t_d, 2\Omega) \propto \sum_v A_v \cos(\omega_v t_d + \varphi_v) \exp(-t_d/T_v) \quad (1)$$

where A_v, ω_v, φ_v, and T_v are the amplitude, frequency, phase, and dephasing time of each vibrational mode.[14,16] The time-domain response $\chi^{(4)}(t_d)$ is Fourier-transformed to a vibrational spectrum $\chi^{(4)}(\omega_v)$. This presentation is analogous to what has been established in time-domain, third-order Raman spectroscopy.[19,20] When the transition from g to e_1 is resonant to the energy of one pump photon, a cosine-like oscillation with $\varphi_v = 0$ or π is generated, as has been observed on GaAs,[12] Cs/Pt,[13] Gd,[15] and an oxazine solution.[14] If the pump photon energy is out of the electronic resonance, a sine-like oscillation with $\varphi_v = \pi/2$ or $3\pi/2$ was expected and was observed on a TiO_2 surface.[16]

The probe light generates two second-harmonic (SH) fields having a wave vector of $2\boldsymbol{k}^{R}_{probe}$, the pump-free SH field and the pump-induced nonoscillatory SH field, in addition to the fourth-order field of $\boldsymbol{k}^{R}_{signal}$ ($= 2\boldsymbol{k}^{R}_{probe}$). The nonoscillatory field $E_{non}(t_d, 2\Omega)$ is ascribed to the ground-state population depleted by the pump irradiation. Time-resolved second-harmonic generation (TRSHG) with picosecond or subpicosecond time resolution has been applied to observe the nonoscillatory field $E_{non}(t_d, 2\Omega)$ from various interfaces.[21−26] The fourth-order field interferes with the two SH fields, and thus the heterodyned detection of the fourth-order Raman component is enabled. The pump-affected 2Ω intensity $I(t, 2\Omega)$ with respect of the pump-free SH intensity $I_0(2\Omega)$ is given by

$$\frac{I(t_d, 2\Omega)}{I_0(2\Omega)} = \frac{|E_0(2\Omega) + E_{signal}(t_d, 2\Omega)|^2}{|E_0(2\Omega)|^2} \quad (2)$$

$E_0(2\Omega)$ denotes the pump-free SH field, and the pump-induced 2Ω field $E_{signal}(t_d, 2\Omega)$ is given in

$$E_{signal}(t_d, 2\Omega) = E_{non}(t_d, 2\Omega) \exp(i\Phi) + E_{fourth}(t_d, 2\Omega) \exp(i\phi) \quad (3)$$

where Φ denotes the phase shift of $E_{non}(t_d, 2\Omega)$ relative to $E_0(2\Omega)$. The phase shift Φ is assumed to be zero because E_{non} and E_0 are generated in a common transition governed by $\chi^{(2)}$. ϕ represents the phase shift of $E_{fourth}(t_d, 2\Omega)$ relative to $E_0(2\Omega)$. With $E_{fourth}(t_d, 2\Omega)$ being much smaller than the other terms, eq 2 is simplified as,

$$E_{fourth}(t_d, 2\Omega)E_0(2\Omega) \propto \frac{I(t_d, 2\Omega) - |E_{SH}(t_d, 2\Omega)|^2}{E_{SH}(t_d, 2\Omega)} E_0(2\Omega) \quad (4)$$

$E_{SH}(t_d, 2\Omega) = E_0(2\Omega) + E_{non}(t_d, 2\Omega)$ is given by fitting the observed $I(t_d, 2\Omega)$ with nonoscillatory numerical functions. The right-hand side of eq 4 is thereby determined by observables, i.e., the 2Ω intensity as a function of the pump−probe delay t_d.[14] The fourth-order Raman response on the left-hand side, proportional to the optical response $\chi^{(4)}(t_d)$, is heterodyned with $E_0(2\Omega)$ and experimentally determined on the right-hand side.

The heterodyned fourth-order Raman signal is expressed with $\chi^{(4)}(t_d)$ as[16]

$$E_{fourth}(t_d, 2\Omega)E_0(2\Omega) \propto \int_{-\infty}^{\infty} dt_2 E_0(t_2 - t_d, 2\Omega) E_{probe}(t_2 - t, \Omega)^2 \times \int_{-\infty}^{t_2} dt_1 |E_{pump}(t_2 - t_1, \Omega)|^2 \chi^{(4)}(t_2 - t_1) \quad (5)$$

where E_{probe} and E_{pump} denote the probe and pump fields. Equation 5 indicates that the instrumental response is given by the temporal profile of the pump-free SH field as a function of time t, $E_0(t, 2\Omega)$, multiplied with the profile of the probe intensity, $E_{probe}(t, 2\Omega)^2$, and then convoluted with the profile of the pump intensity, $|E_{pump}(t, 2\Omega)|^2$. The validity of eq 5 has been confirmed on a TiO_2 surface.[16]

3. Experimental Section

3.1. Fourth-Order Raman Spectrometer. Our spectrometer based on a sub-20-fs laser system is illustrated in Figure 1b. A noncollinear optical parametric amplifier (TOPAS-white, Quantronix) was pumped by a Ti:sapphire regenerative amplifier (Hurricane, Spectra Physics, 800 nm, 90 fs, 1-kHz repetition rate). The ultraviolet radiation emitted from the parametric amplifier was blocked with a long-wavelength-pass dielectric filter (filter 1, substrate: 1-mm-thickness synthetic quartz, Asahi

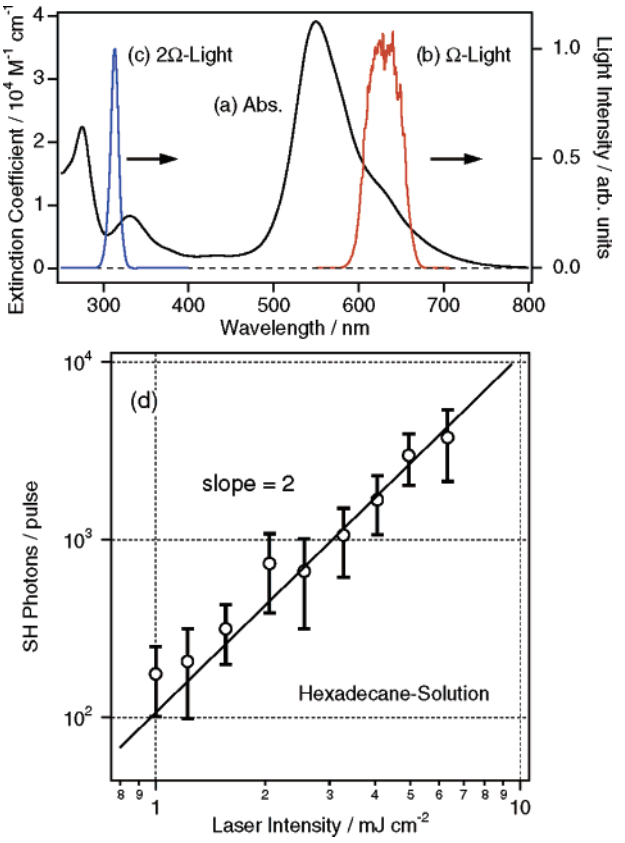

Figure 2. (a) Steady-state absorption spectrum of oxazine 170 in an aqueous solution (0.2 mmol L^{-1}) containing NaCl (0.1 mol L^{-1}). The spectrum of (b) the pump and probe light pulses and (c) the second-harmonic light generated at the hexadecane−solution interface. The intensity of the second-harmonic light at the hexadecane−solution interface is plotted in (d) as a function of the incident light intensity.

Spectra). The wavelength of the pump and probe pulses was tuned at 630 nm to be resonant with the electronic absorption of oxazine 170. Figure 2 shows the steady-state absorption spectrum of oxazine 170 and the spectrum of the tuned light pulse. The tuned output (∼10 μJ) was divided to pump and probe lights with a dielectric beam splitter (03BTF001, Melles Guriot, substrate: 1-mm-thickness BK7) and attenuated with variable neutral-density filters (VND-50U, Sigma Koki, substrate: 2-mm-thickness synthetic quartz). The pump−probe delay t_d was controlled by a computer-driven translational stage (KS102−70A, Suruga Seiki) with a resolution of 0.067 fs $step^{-1}$. The full width at half-maximum (fwhm) of the pump and probe intensities (τ_{pu-pr}) was determined to be 17.3 fs by using a SH signal observed with a 50-μm-thick β-BaB_2O_4 (BBO) crystal (Castech) on the assumption that the pulse shape was a Gaussian function.

The *p*-polarized pump (5 mJ cm^{-2}) and *p*-polarized probe (2.5 mJ cm^{-2}) beams were focused with a concave mirror (10DC500ER.1, Newport, r = 500 mm) and crossed on the hexadecane−solution interface at a crossing angle of 2° with an incident angle of $\theta \sim 50°$ for the probe beam. The spot diameter of the beams was 0.1 mm. The *p*-polarized 2Ω frequency light (wavelength: 315 nm) emitted to the reflected direction was detected with a photomultiplier tube (PMT, H5784-03, Hamamatsu), while the reflected probe light of Ω frequency was blocked with a short-wavelength-pass filter (filter 2, substrate: 1-mm-thickness synthetic quartz, Asahi Spectra). The total transmittance of the Glan−Taylor polarizer (03PTA403, Melles Griot), filter 2, and mirrors was 0.52. The output of PMT was gated with a boxcar integrator (SR250, Stanford Research System), A/D converted (SR245, Stanford Research System), and sent to a PC on a pulse-to-pulse basis. The pump pulse was chopped at 500 Hz with a synchronous mechanical chopper (3501, New Focus). The pump-on signal and pump-off signal were separately accumulated, and the former was divided by the latter. The time origin ($t_d = 0$) was determined by monitoring the SH light intensity emitted from the target interface. The hexadecane layer covering the interface induced GVD in the light pulses. The GVD was compensated by adding an extra negative charp by the grating pulse compressor built in the TOPAS-white. The fwhm of the instrumental response observed at the hexadecane−solution interface was minimized to 23 fs by adjusting the compressor. The minimized response (23 fs) determined the spectral sensitivity in the frequency domain to be a Gaussian function having a half width at half-maximum (hwhm) of 640 cm^{-1} centered at 0 cm^{-1}. The wavenumber resolution of the Fourier transformed spectrum is given by a Gaussian function having an fwhm of 6 cm^{-1}. Details are described in Sections 4.2 and 4.5.

3.2. Dye Solution. Oxazine 170 (99%, Acros) was dissolved in HPLC-grade water (Wako) at a concentration of 0.2 mmol L^{-1}. Sodium chloride (0.1 mol L^{-1}) was added to the solution to enhance the SH intensity.[27] Hexadecane (99+%, anhydrous, Aldrich) was put on the oxazine solution with a thickness of 0.2 mm. The dye was not soluble in hexadecane at all.

3.3. Spontaneous Raman Measurements. Spontaneous Raman spectra of an oxazine solution of the same concentration (0.2 mmol L^{-1}) with sodium chloride (0.1 mol L^{-1}) and solid oxazine were measured with a Raman spectrometer (NRI-1866M, JASCO) composed of a subtractive double monochromator, a single polychromator, and a CCD detector. A 514.5-nm line of a CW argon-ion laser was used for the excitation of Raman spectra. The excitation intensity was 2 mW at the sample position. Accumulation time of a spectrum was 100 s with a frequency resolution of 3 cm^{-1}.

4. Results and Discussion

4.1. Pump-Free SH Generation. First, the pump-free SH generation at the hexadecane−solution interface was examined. The spectrum of the SH light emitted from the interface reproduced the SH spectrum observed with a 50-μm-thick BBO crystal as shown in Figure 2c. The SH light intensity of the interface was proportional to the squared probe intensity, as expected (Figure 2d). The SH generation at an air−hexadecane interface was negligible. Thus, the pump-free SH generation definitely occurred at the hexadecane−solution interface.

4.2. Instrumental Response of Fourth-Order Raman Spectrometer. The hexadecane−solution interface and the air−solution interface were irradiated with pump and probe pulses to determine the time origin (t_d = 0) and the instrumental response. The intensity of the reflected SH light having a wave vector of $\boldsymbol{k}_{SH}^{R} = \boldsymbol{k}_{pump}^{R} + \boldsymbol{k}_{probe}^{R}$ was measured as a function of the pump−probe delay and plotted in Figure 3a and b. The transmitted SH light of a 50-μm-thick BBO crystal having $\boldsymbol{k}_{SH} = \boldsymbol{k}_{pump} + \boldsymbol{k}_{probe}$ was also observed and is shown in Figure 3c. The FWHMs of three profiles (a: hexadecane−solution interface, b: air−solution interface, and c: BBO crystal) were 30.5, 29.0, and 24.4 fs, respectively. The timewidth on the air−solution interface was broadened relative to the timewidth of the BBO crystal. This is because of the finite lifetime of the superposition state $|e_1\rangle\langle g|$. The population lifetime of the e_1 state, the dephasing of $|e_1\rangle\langle g|$, and the inhomogeneity of the $|e_1\rangle\langle g|$ ensemble can affect the lifetime of the superposition state $|e_1\rangle\langle g|$.

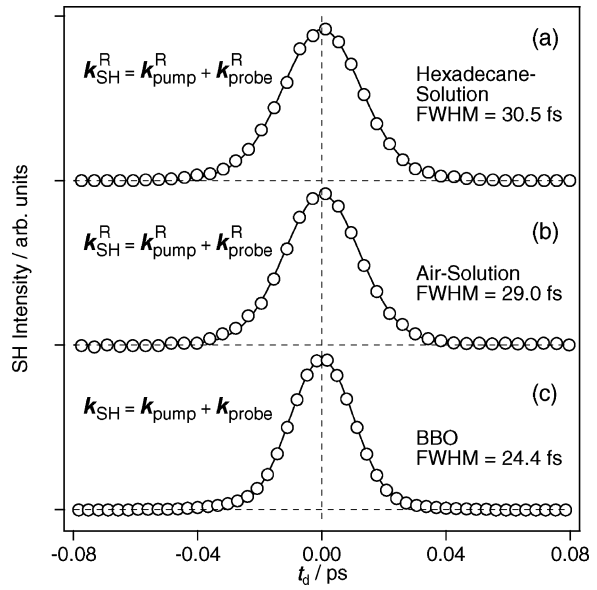

Figure 3. Temporal profile of the reflected noncollinear second-harmonic light generated at (a) the hexadecane−solution and (b) air−solution interface irradiated with pump and probe pulses (open circles). Solid lines in (a) and (b) present fitting to eq 6. Open circles in (c) shows the profile of the transmitted noncollinear second-harmonic light generated in a 0.5-mm-thick β-BaB_2O_4 crystal. Fitting to a Gaussian function is shown with the solid line.

Assume the superposition state exponentially decayed with a time constant τ_{D1}. The profile of the SH intensity is expressed as

$$S_{SHG}(t_d) \propto |s(t_d) + s(-t_d)|^2$$

$$\text{with } s(t_d) = \int_{-\infty}^{\infty} dt_2 E(t_2 - t_d) \int_{-\infty}^{t_2} dt_1 E(t_1) R(t_2 - t_1),$$

$$R(t) = A \exp(-t/\tau_{D1}) \quad (6)$$

The temporal behaviors of the pump and probe lights $E(t)$ were assumed to be a Gaussian function having fwhms of $\sqrt{2}\tau^{air}_{pu-pr}$ ($\sqrt{2}\tau^{hexadecane}_{pu-pr}$) on the air−solution (hexadecane−solution) interface. The pulse width at the air−solution interface τ^{air}_{pu-pr} should have been equal to the width determined with the BBO crystal ($\tau_{pu-pr} = 17.3$ fs) because the pulses traveling in air experience little GVD. The profile observed on the air−solution interface was fitted by eq 6 with $\tau_{D1} = 8.5$ fs. The fitting result is shown by a solid curve of Figure 3b. The exponential decay function with $\tau_{D1} = 8.5$ fs in the time domain corresponds to a Lorentz function of an fwhm of 1200 cm^{-1} in the frequency domain. Yamaguchi and Tahara[28] determined the energy width of the first excited state e_1 of a similar dye (Nile Blue) placed at an air−solution interface to be 1400 cm^{-1}. Our estimation is close to their number. The other feature of eq 6 is the maximum of the SH intensity at the time origin, zero delay. Fourth-order Raman measurements described in the following sections were done with the time origin determined in the noncollinear SH generation at the interface on trial.

The fwhm of the hexadecane−solution interface was still broader by 5% than that of the air−solution interface. This excess broadening is attributed to the residual GVD in the hexadecane layer. Actually, the extent of the broadening exhibited a positive relationship with the thickness of the hexadecane layer. A finite dispersion resided in the pulses having passed through the liquid layer, although the time width of the SH intensity at the interface was minimized. If τ_{D1} is constant to be 8.5 fs at the hexadecane−solution interface, the fwhm of the pump and probe pulses at the interface $\tau^{hexadecane}_{pu-pr}$ is estimated to be 18.3 fs by using eq 6. The fitting curve is shown in Figure 3a.

The instrumental response is evaluated at the hexadecane−solution interface and air−solution interface by using eq 5.[16] We need the temporal profile of $E_0(2\Omega)$ to do so. The time width of $E_0(2\Omega)$ is broader than the width of squared $E_{probe}(\Omega)$ due to the lifetime broadening coming from the superposition state $|e_2\rangle\langle g|$ (see Figure 1a). Yamaguchi and Tahara[28] observed electronically resonant sum-frequency spectrum of Nile Blue and found the e_2 band to be a Lorentz function having an fwhm of 1000 cm^{-1}. The bandwidth corresponds to an exponential decay having a time constant $\tau_{D2} = 11$ fs. Assuming an exponential decay having $\tau_{D2} = 11$ fs at our interfaces, the fwhm of $E_0(2\Omega)$ is estimated from the convolution of the 11-fs decay and the pulse widths to be 23 fs at the hexadecane−solution interface and 22 fs at the air−solution interface. On the basis of eq 5, the fwhm of the instrumental response, τ_{inst}, is finally predicted to be 23 fs at the hexadecane−solution interface and 22 fs at the air−solution interface.[14,16,19,29]

4.3. Fourth-Order Raman Response. The normalized intensity of the 2Ω light, $I(t_d, 2\Omega)/I_0(2\Omega)$, on the hexadecane−solution interface is shown as a function of t_d in Figure 4a. The signal having a wave vector of $k^R_{pump} - k^R_{pump} + k^R_{probe}$ was measured. The SH intensity was instantaneously decreased by the pump irradiation and recovered monotonically in picoseconds. Periodic oscillation, which represents fourth-order Raman response, was superimposed on the recovering trace. The decrease and recovery were observed on a number of air−liquid interfaces, recognized as TRSHG, and interpreted with the electronic ground-state population depleted by the pump irradiation and restored.[21−25] We follow the received picture to interpret our result of the hexadecane−solution interface. The recovery in the range of 0−5 ps was fitted to a four-term multiexponential function convoluted with the instrumental response (a Gaussian function having an fwhm of 23 fs). The time constants τ_i and the amplitudes A_i of the four exponential terms were $\tau_1 < \tau_{inst}$, $\tau_2 = 0.220 \pm 0.008$ ps, $\tau_3 = 2.2 \pm 0.1$ ps, $\tau_4 > 5$ ps, $A_1 = -0.384 \pm 0.006$, $A_2 = -0.231 \pm 0.004$, $A_3 = -0.221 \pm 0.002$, and $A_4 = -0.146 \pm 0.003$. Figure 4c shows the trace observed on the air−solution interface, which was similarly fitted with $\tau_1 < \tau_{inst}$, $\tau_2 = 0.208 \pm 0.008$ ps, $\tau_3 = 2.3 \pm 0.1$ ps, $\tau_4 > 5$ ps, $A_1 = -0.503 \pm 0.007$, $A_2 = -0.259 \pm 0.005$, $A_3 = -0.219 \pm 0.003$, and $A_4 = -0.137 \pm 0.004$. Each set of τ_i and A_i was comparable at the two interfaces, suggesting a similar local structure of solvent (water) surrounding the oxazine chromophore.

The multiexponential function reproduced the nonoscillatory TRSHG component. The oscillatory component was then deduced from the raw data by using eq 4. The deduced oscillations, which correspond to the heterodyned fourth-order Raman response of $E(t, 2\Omega)E_0(2\Omega)$, are shown in Figure 4b and d. The responses exhibit damped oscillation with several vibrational frequencies, ω_v, as expressed in eq 1.

4.4. Third-Order Raman Response. The time-resolved reflectance change of the probe light was monitored at the air−solution interface to obtain the bulk-sensitive, third-order Raman response of the oxazine solution.[30] An undesired optical cascade may have generated the SH oscillations. The possible contribution of the cascade is considered and excluded in Section 4.6 on the basis of the third-order response observed here. The normalized reflectance, $R(t_d, \Omega)/R_0(\Omega)$, was monitored with pulse energy, polarization, and incidence angle in the same manner as that for the operation of Figure 4. The reflectance

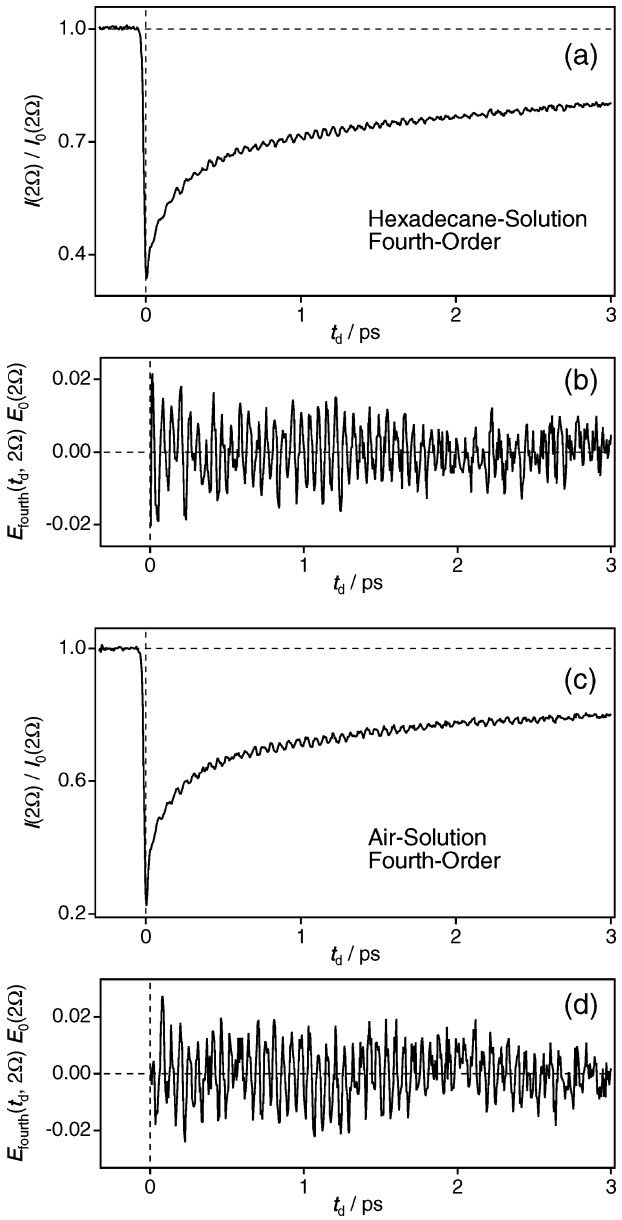

Figure 4. Second-harmonic light intensity observed at (a) the hexadecane−solution interface and at (c) the air−solution interface as a function of the pump−probe delay. Excitation wavelength: 630 nm; incident angle θ: 50°. Response to 14 000 probe pulses were averaged to get one data point. Oscillations deduced from each trace are shown in (b) and (d). They are ascribed to the fourth-order Raman responses. The signals having a wave vector of $k^{R}_{pump} - k^{R}_{pump} + 2k^{R}_{probe}$ were measured.

shown in Figure 5a contains nonoscillatory and oscillatory components. The former comes from the depleted ground state of the dye[14,26] and was fitted in the range of 0−5 ps to a multiexponential function having a $\tau_1 < \tau_{inst}$, $\tau_2 = 0.058 \pm 0.005$ ps, $\tau_3 = 0.23 \pm 0.01$ ps, $\tau_4 > 5$ ps, $A_1 = -0.0084 \pm 0.0003$, $A_2 = -0.0138 \pm 0.0007$, $A_3 = -0.0081 \pm 0.0008$, and $A_4 = +0.00009 \pm 0.00001$. Reflectance oscillations due to the impulsive stimulated Raman scattering[14,19,29,31] was deduced in Figure 5b by subtracting the fitted function from the raw reflectance.

The two sets of time constants deduced from the third-order and fourth-order responses cannot be directly compared. The amplitude of the nonoscillatory component due to a transient absorption, $E_{non}(t_d, \Omega)$, was much smaller than the electric field of the reflected probe light $E_0(\Omega)$. $E_{non}(t_d, \Omega)$ was heterodyned

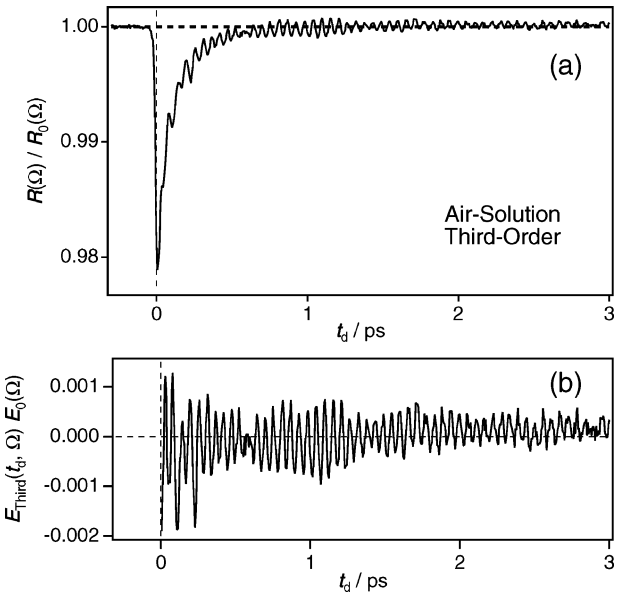

Figure 5. Reflectance change of the air−solution interface as a function of the pump−probe delay (a). Reflectance oscillations deduced by subtracting the fitted function is shown in (b). They are ascribed to the third-order Raman responses.

to be linear to the reflectance change. In contrast, the pump-free second-harmonic field, $E_0(2\Omega)$, was in the same order of the pump-induced nonoscillatory component of the second-harmonic field, $E_{non}(t_d, 2\Omega)$. The observed response of the second-harmonic light intensity contains the homodyned contribution, $|E_{non}(2\Omega)|^2$, and the heterodyned response proportional to $E_{non}(t_d, 2\Omega)$. The time constants in the fourth-order response do not reproduce the rate constants of postphotoexcitation processes of the dye.

The sign of the nonoscillatory component was negative, as shown in Figure 5a. This is opposed to the positive sign observed in our previous work[14] on the same air−solution interface.[32] The inversion of the reflectance change is understood with the phase of the reflected light field shifted at the interface.[29] The phase shift of the *p*-polarized reflected light with respect to the incident light is $\pi(0)$, with the incident angle smaller (larger) than the Brewster angle of the interface θ_B. Reflectance change in Figure 5a was observed with $\theta = 50°$, which is less than $\theta_B = 56°$. On the other hand, the previous measurement[14] was done at $\theta = 65°$. The phase shift by π caused the inverted response of the reflected light intensity.

4.5. FT Spectrum of Fourth-Order Raman Response. Figure 6 presents the FT spectrum of the two fourth-order and one third-order Raman responses. The oscillatory component at 0−5 ps was multiplied by a window function, a Gaussian function having a hwhm of 2.5 ps centered at $t_d = 0$ and connected to null data points inserted at 5−50 ps. The modified response was Fourier-transformed to give the frequency spectrum. Multiplying the window function corresponds to convoluting a raw FT spectrum with a Gaussian function having a 6 cm^{-1} fwhm. The frequency resolution is thereby determined to be 6 cm^{-1} in the current measurements. Relative sensitivity at different wavenumbers is, on the other hand, given by the Fourier transformation of the instrumental response function.[19,20,33] The response at the hexadecane−solution (air−solution) interface, a Gaussian function with an fwhm of 23 (22) fs, leads to a Gaussian sensitivity curve centered at 0 cm^{-1} with a hwhm of 640 (670) cm^{-1}. The FT spectra are presented in Figure 6 without correcting the wavenumber-dependent sensitivity.

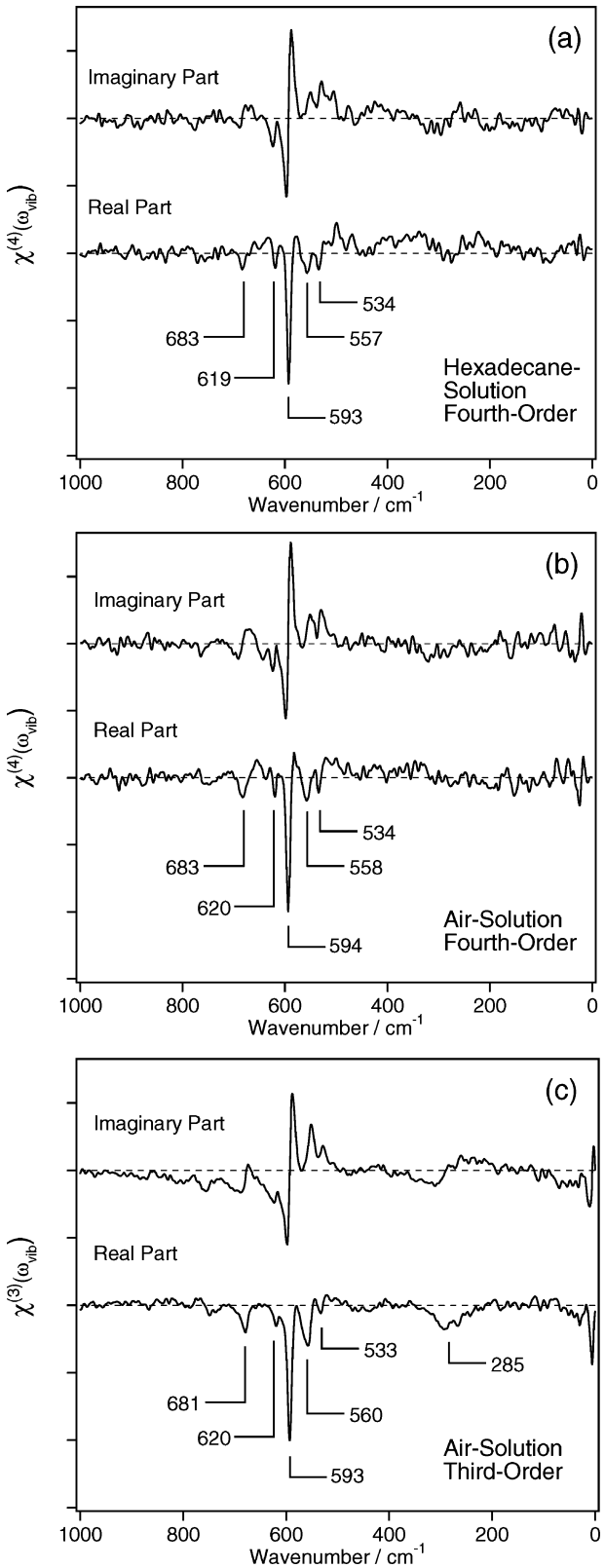

Figure 6. Fourier-transformed spectra of the fourth-order Raman response observed on (a) the hexadecane−solution and (b) air−solution interfaces. Real part and imaginary part of the spectra are shown. Fourier-transformed spectrum of the third-order Raman response on the air−solution interface is presented in (c). The frequency resolution was a Gaussian function of a 6 cm^{-1} fwhm.

On the FT spectrum of the fourth-order Raman response at the hexadecane−solution interface, symmetrically shaped bands having the negative signs were identified at 534, 557, 593, 619, and 683 cm^{-1} in the real part of the FT spectrum, together with dispersively shaped bands at the corresponding wavenumbers in the imaginary part. The observed band shape indicates the phase of the vibrational coherence, φ_v, to be π in eq 1. Hence the Raman pump process is one-photon resonant to an electronic exciation.[12−14] The FT spectrum of the hexadecane−solution interface reproduced the spectrum of the air−solution interface in center wavenumbers and also band shapes. This suggests that the observed modes of vibration were insensitive to the composition of the interface.

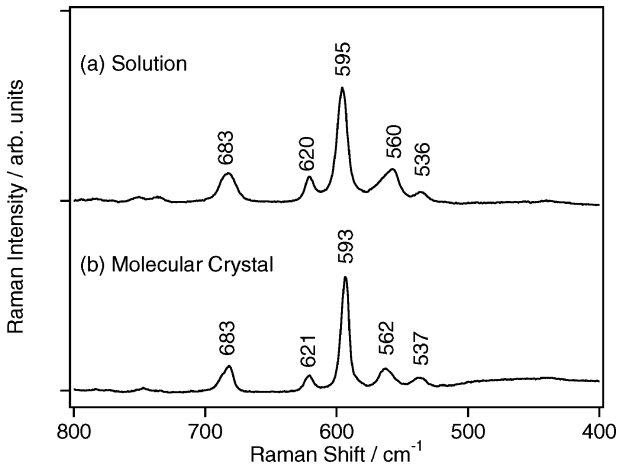

Figure 7. Spontaneous resonance Raman spectra of (a) the oxazine solution and (b) oxazine solid.

The spontaneous Raman spectrum of oxazine 170 was observed in the bulk solution and in bulk solid to support the vibrational bands insensitive to environments. Dye monomers are equilibrated with dimerized species in the solution.[26−28] The solvated monomer, solvated dimer, and molecules in solid are in different dielectric environments and experience different intermolecular interactions. The observed Raman bands are nevertheless identical with each other, as shown in Figure 7. It is hence not surprising that the vibrational bands observed by fourth-order Raman scattering are insensitive to the hexadecane layer covering the interface. The solvent structure in the vicinity of chromophores is sometimes sensitive to the interface composition, though.[5,34−36]

4.6. Exclusion of an Undesired Optical Transition. In addition to the desired fourth-order Raman response, the possible contribution of an undesired optical transition is considered and excluded. Two independent third-order Raman processes sometimes cascade one after the other, and the resulting emission of light is misidentified to be generated in a fifth-order Raman scattering.[37,38] The consideration has been outlined in our previous paper.[14] The full description is presented here.

The optical cascade possible at our interface is illustrated in Figure 8. A third-order Raman scattering due to $\chi^{(3)}$ of compound A occurs in the bulk solution, and the SH generation due to $\chi^{(2)}$ of compound B may be coupled at the interface. The electric field due to $\chi^{(3)}$ of A, $E_{third}(t_d, \Omega)$, propagates to the interface and modulates the probe field, $E_{probe}(\Omega)$. The SH light is generated on the modulated probe field, $E_{probe}'(t_d, \Omega)$. The SH light intensity affected by the cascade is given in

$$I_{cascade}(t_d, 2\Omega) = |E_{SH}(t_d, 2\Omega)|^2 = |\chi^{(2)}|^2 |E_{probe}'(t_d, \Omega)|^4 = |\chi^{(2)}|^2 |E_{probe}(\Omega) + E_{third}(t_d, \Omega)\, e^{i\psi}|^4 \quad (7)$$

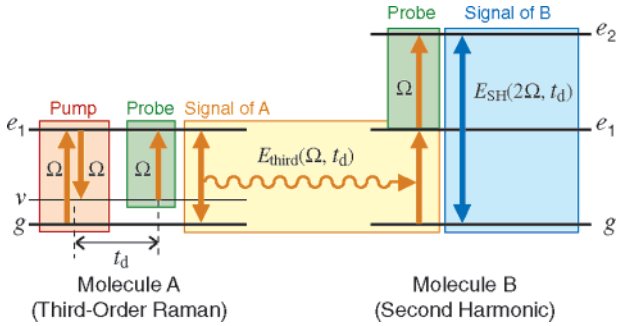

Figure 8. An optical cascade composed of the third-order Raman transition in the bulk and the second-harmonic generation at the interface, excluded in the present system.

with ψ as the phase shift of E_{probe} relative to E_{third}. Assuming $|E_{third}| \ll |E_{probe}|$, the cascade-induced term is approximated as

$$\frac{I_{cascade}(t_d, 2\Omega)}{I_0(2\Omega)} \sim 1 + \frac{4E_{third}(t_d, \Omega)\cos\psi}{E_{probe}(\Omega)} \quad (8)$$

E_{third} radiating to the reflected direction is averaged to be nearly zero when integrated over the solution of a macroscopic dimension because of the phase-match requirement. Compound A contained in the thin solution layer of a thickness comparable with the probe wavelength (630 nm) can still contribute to E_{third}, being free from the phase-match requirement. Suppose that the optical transmittance of the thin solution layer is observed as a function of the time delay. The transmittance change of the thin layer ΔT_{thin} is given in,

$$\Delta T_{thin}(t_d, \Omega) \sim \frac{2E_{third}(t_d, \Omega)\cos\psi}{E_{probe}(\Omega)} \quad (9)$$

and thus

$$\frac{I_{cascade}(t_d, 2\Omega)}{I_0(2\Omega)} \sim 1 + 2\Delta T_{thin}(t_d, \Omega) \quad (10)$$

We estimate ΔT_{thin} based on the amplitude of the reflectance oscillation (ΔR), though ΔT_{thin} is difficult to observe at the interface. The transmittance and reflectance are related in[29,39]

$$\Delta T_{thin}(t_d, \Omega) = \frac{E_{R0}(\Omega)}{E_{probe}(\Omega)}\Delta R(t_d, \Omega) \quad (11)$$

where E_{R0} denotes the reflected probe field. On our air−solution interface, $|E_{R0}/E_{probe}|$ is calculated to be 0.05 on the basis of a Fresnel equation. The observed magnitude of $|\Delta R|$ was 0.001 in Figure 5b, yielding $2|\Delta T_{thin}|$ as small as 0.0001. The oscillation amplitude of the SH intensity in Figure 4d (∼0.02) was larger by 2 orders of magnitude than the estimated amplitude of the cascade-induced oscillation. The current estimation is in good agreement with the estimation done on the same interface with a different probe wavelength (600 nm) and a different incident angle ($\theta = 65°$).[14] A frequency-domain detection of fourth-order Raman response was recently done on an air−solution interface, and the fraction of the cascade-induced response was estimated to be 10^{-8} or less.[18]

Additional experimental evidence supports the exclusion of the cascade-induced oscillations. Equation 8 requires that the FT spectrum of the cascade process reproduces the spectrum of the third-order Raman spectrum. If the oscillations of SH intensity were generated by the cascade, the FT spectrum of Figure 6b would exactly reproduce the spectrum of Figure 6c. This is not the case. Six bands at 285, 533, 560, 590, 620, and 681 cm^{-1} appeared in the third-order Raman spectrum of Figure 6c. The relative intensities of 285 cm^{-1} and 533 cm^{-1} bands in Figure 6c are different from those of Figure 6a and b. These differences suggest, on the finite signal-to-noise ratio in the observed FT spectra, that the observed SH light oscillations are free from the contribution of the cascade. The cross section of the fourth-order transition is proportional to the product of the Raman tensor (α) and hyper-Raman tensor (β), whereas the probability of the third-order transition is proportional to $|\alpha|^2$.[14] α and β of the two vibrational bands are naturally independent, leading to the different band intensities of third-order and fourth-order responses.

We thus quantitatively estimated the cascade-induced response to be far less intense than the fourth-order response. One reason of this is the small thickness of the solution layer penetrated by the pump light pulse. Because the pump light is reflected at the interface, the penetration depth is comparable to the wavelength. The intensity of third-order Raman scattering, the initial stage of the cascade, is positively dependent on the volume of the penetration layer.

5. Conclusions

The feasibility of the time-domain, fourth-order Raman spectroscopy was demonstrated by observing molecular vibrations at a liquid−liquid interface. The group velocity dispersion of the pump and probe light pulses were corrected to optimize the instrumental response to be 23 fs in fwhm. Oxazine 170 located at a hexadecane−solution interface exhibited five bands at 534, 557, 593, 619, and 683 cm^{-1}. The possible contribution of an undesired, bulk-sensitive optical response was estimated to be smaller by 2 orders of magnitude than the contribution of the desired, interface-selective response.

When fourth-order Raman spectroscopy is compared with sum-frequency spectroscopy, vibrational coherence is excited by a Raman transition in the former instead of an IR transition in the latter. Interfaces buried in IR-absorbing media come in the observable range. Access to low-wavenumber vibrations, including frustrated modes and intermolecular modes, is opened. The two major advantages promise a new frontier of interface chemistry to be explored.

Acknowledgment. We are pleased to acknowledge fruitful discussions with S. Yamaguchi of Riken and Y. R. Shen of the University of California−Berkeley. The present work is supported by a grant-in-aid for scientific research (KAKENHI) in priority area "molecular nanodynamics" from Ministry of Education, Culture, Sports, Science, and Technology. The spontaneous Raman spectra were measured at the Natural Science Center for Basic Research and Development (N-BARD), Hiroshima University.

References and Notes

(1) Shen, Y. R. *The Priciple of Nonlinear Optics*; Wiley-Interscience: New York, 1984.
(2) Shen, Y. R. *Nature* **1989**, *337*, 519.
(3) Eisenthal, K. B. *Chem. Rev.* **1996**, *96*, 1343.
(4) Miranda, P. B.; Shen, Y. R. *J. Phys. Chem. B* **1999**, *103*, 3292.
(5) Scatena, L. F.; Brown, M. G.; Richmond, G. L. *Science* **2001**, *292*, 908.
(6) Roke, S.; Schins, J.; Müller, M.; Bonn, M. *Phys. Rev. Lett.* **2003**, *90*, 128101.
(7) Wang, J.; Even, M.; Chen, X.; Schmaier, A. H.; Waite, J. H.; Chen, Z. *J. Am. Chem. Soc.* **2003**, *125*, 9914.
(8) Ishibashi, T.; Onishi, H. *Appl. Spectrosc.* **2002**, *56*, 1298.
(9) Ishibashi, T.; Onishi, H. *Appl. Phys. Lett.* **2002**, *81*, 1338.

(10) Ishibashi, T.; Uetsuka, H.; Onishi, H. *J. Phys. Chem. B* **2004**, *108*, 17166.
(11) Uosaki, K.; Yano, T.; Nihonyanagi, S. *J. Phys. Chem. B* **2004**, *108*, 19086.
(12) Chang, Y. M.; Xu, L.; Tom, H. W. K. *Phys. Rev. Lett.* **1997**, *78*, 4649.
(13) Watanabe, K.; Takagi, N.; Matsumoto, Y. *Chem. Phys, Lett.* **2002**, *366*, 606.
(14) Fujiyoshi, S.; Ishibashi, T.; Onishi, H. *J. Phys. Chem. B* **2004**, *108*, 10636.
(15) Bovensiepen, U.; Melnikov, A.; Radu, I.; Krupin, O.; Starke, K.; Wolf, M.; Matthias, E. *Phys. Rev. B* **2004**, *69*, 235417.
(16) Fujiyoshi, S.; Ishibashi, T.; Onishi, H. *J. Phys. Chem. B* **2005**, *109*, 8557.
(17) Hirose, Y.; Yui, H.; Sawada, T. *J. Phys. Chem. B* **2005**, *109*, 13063.
(18) Yamaguchi, S.; Tahara, T. *J. Phys. Chem. B* **2005**, *109*, 24211.
(19) Ziegler, L. D.; Fan, R.; Desrosiers, A. E.; Scherer, N. F. *J. Chem. Phys.* **1994**, *100*, 1823.
(20) Cho, M.; Du, M.; Scherer, N. F.; Fleming, G. R.; Mukamel, S. *J. Chem. Phys.* **1993**, *99*, 2410.
(21) Meech, S. R.; Yoshihara, K. *Chem. Phys, Lett.* **1990**, *174*, 423.
(22) Meech, S. R.; Yoshihara, K. *J. Phys. Chem.* **1990**, *94*, 4913.
(23) Castro, A.; Sitzmann, V.; Zhang, D.; Eisenthal, K. B. *J. Phys. Chem.* **1991**, *95*, 6752.
(24) Antoine, R.; Tamburello-Luca, A. A.; Hebért, P.; Brevet, P. F.; Girault, H. H. *Chem. Phys. Lett.* **1998**, *288*, 138.
(25) Zimdars, D.; Dadap, J. I.; Eisenthal, K. B.; Heinz, T. F. *Chem. Phys, Lett.* **1999**, *301*, 112.
(26) Steinhurst, D. A.; Baronavski, A. P.; Owrutsky, J. C. *J. Phys. Chem. B* **2002**, *106*, 3160.
(27) Steinhurst, D. A.; Owrutsky, J. C. *J. Phys. Chem. B* **2001**, *105*, 3062.
(28) Yamaguchi, S.; Tahara, T. *J. Phys. Chem. B* **2004**, *108*, 19079.
(29) Fujiyoshi, S.; Ishibashi, T.; Onishi, H. *J. Phys. Chem. B* **2004**, *108*, 1525.
(30) The number of oxazine molecules, which generate the fourth-order Raman response, is 1×10^{14} cm^{-2} when the hexadecane−solution interface is fully covered with the dye of 1 nm^2 molecule^{-1}. Assuming the penetration depth of the probe light to be 1 μm, the thin solution layer responsible for reflecting the light contains 1×10^{13} dye-molecules cm^{-2}. The observed third-order Raman response is therefore originated from the dye molecules exposed to the interface and by those in the solution layer to a comparable extent.
(31) Joo, T.; Jia, Y.; Yu, J.-Y.; Lang, M. J.; Fleming, G. R. *J. Chem. Phys.* **1996**, *104*, 6089
(32) The sign of the oscillations is also opposite of the results of the previous study[14] because of the same reason. The symmetric bands to the negative sign in Figure 6c show $\varphi_v = \pi$. Positive symmetric peaks were observed in the previous study, leading to $\varphi_v = 0$.
(33) Fujiyoshi, S.; Takeuchi, S.; Tahara, T. *J. Phys. Chem. A* **2003**, *107*, 494.
(34) Shi, X.; Borguet, B.; Tarnovsky, A. N.; Eisenthal, K. B. *Chem. Phys.* **1996**, *205*, 167.
(35) Uchida, T.; Yamaguchi, A.; Ina, T.; Teramae, N. *J. Phys. Chem. B* **2000**, *104*, 12091.
(36) Knock, M. M.; Bell, G. R.; Hill, E. K.; Turner, H. J.; Bain, C. D. *J. Phys. Chem. B* **2003**, *107*, 10801.
(37) Kirkwood, J. C.; Ulness, D. J.; Albrecht, A. C.; Stimson, M. J. *Chem. Phys, Lett.* **1998**, *293*, 417.
(38) Kano, H.; Hamaguchi, H. *J. Chem. Phys.* **2003**, *118*, 4556.
(39) Fujiyoshi, S.; Ishibashi, T.; Onishi, H. *J. Mol. Struct.* **2005**, *735*−*736*, 169.